ADVANCED MATERIALS INTERFACES
www.advmatinterfaces.de

Fabrication of Non-Uniform Nanolattices with Spatially Varying Geometry and Material Composition

*I-Te Chen, Zijian Dai, Dennis T. Lee, Yi-An Chen, Gregory N. Parsons, and Chih-Hao Chang**

The fabrication of periodic 3D nanostructures with uniform material properties has been widely investigated and is important for applications in photonics, mechanics, and energy storage. However, creating nanostructures with spatially varying lattice geometry and material composition is still largely an unexplored challenge in nanofabrication. This work presents the fabrication of non-uniform nanolattices by patterning multiple layers of 3D nanostructures using phase shift lithography and atomic layer deposition. By controlling the processing parameters, the lattice geometry and material composition of each individual nanolattice layer can be tailored to create arbitrary material property profiles. Using the proposed method, a five-layer nanolattice with spatially varying porosity and oxide materials has been demonstrated. This process can be used to create gradient-index antireflection nanostructures, and a fabricated four-layer nanolattice structure consisting of TiO_2 and Al_2O_3 with gradually varying porosity reduces more than 90% of the specular reflectance from a silicon substrate. By enabling nanolattices with arbitrary profiles in physical properties, the demonstrated technique can find broad applications in nanophotonics, graded filters, energy storage systems, and nanoarchitected films.

1. Introduction

3D nanostructures have attracted great attention in recent years according to the unique properties observed in materials with nanoscale features. For example, ordered 3D nanostructures with high porosity can have high specific strength and stiffness at low density.[1–7] They also have high surface-to-volume ratio, which is advantageous for energy storage devices.[8–10] Their periodic modulation can also be used to tailor wave behavior in photonic/phononic crystals.[11–15] Various parallel fabrication techniques have been developed for 3D nanostructures with homogeneous properties, such as holographic lithography,[16,17] phase-shift lithography,[14,15,18–23] and nanospheres self-assembly.[24–26] Polymer nanostructures can also be employed as the sacrificial template for thin-film deposition to fabricate hollow-core nanolattices. These periodic architectures with thin-shell elements can have even lower density, demonstrating interesting properties such as lower thermal conductivity,[27] refractive index closer to air,[21] higher mechanical stiffness, and resilience at high strain.[1] These recent progress in the fabrication of 3D nanostructure have provided new opportunity in nanoscience and nanoengineering.

Beyond uniform nanolattices, 3D nanostructures with spatially varying geometry and/or material composition can further enable the control of the material properties. For example, aerogel with gradient porosity was used to capture and spatially separate high-speed particles of different sizes from comets during the NASA Stardust mission.[28,29] Nanostructures with changing lattice geometry can also be used to create complex profiles for nanophotonic and acoustic devices.[1,30–32] Analogous to the recent interest in metasurfaces with spatially varying properties,[33,34] the ability to create non-uniform nanolattices can enable material behavior to be tailored within the full 3D volume.

Fabrication of 3D nanostructures or nanolattices with spatially varying parameters is extremely challenging, and most existing processes are limited to uniform nanostructures. Methods to stack layers of nanostructures[35–37] have been explored, but are restricted in simple geometry such as 1D or 2D grating layers that are strong enough to survive the mechanical transferring process. Direct-write approaches such as two-photon polymerization and focused-ion beam lithography have the capability for arbitrary 3D patterning.[1,7,27,31,32,38] Varying the material composition is possible in these techniques,[39] however the voxel-by-voxel writing methods are serial in nature and can be prohibitively expensive to scale for large-area patterning. There are two key challenges to fabricate non-uniform nanolattices. The first challenge is creating nanostructures with various lattice geometry and periodicity in a scalable manner. This is difficult for existing lithography and self-assembly that are parallel, which are limited to making structures with a single periodicity. The second challenge is altering the material composition as a function of position. The existing deposition methods coat uniformly on the structure surface and it is difficult to selectively deposit in isolated regions. To further

I-T. Chen, Y.-A. Chen, Prof. C.-H. Chang
Walker Department of Mechanical Engineering
The University of Texas at Austin
Austin, TX 78712, USA
E-mail: chichang@utexas.edu
Dr. Z. Dai, D. T. Lee, Prof. G. N. Parsons
Department of Chemical and Biomolecular Engineering
North Carolina State University
Raleigh, NC 27695, USA

The ORCID identification number(s) for the author(s) of this article can be found under https://doi.org/10.1002/admi.202100690.

DOI: 10.1002/admi.202100690

extend the advances of 3D nanostructures, more advanced techniques for creating and controlling non-uniform nanolattices are needed.

Here, we demonstrate a scalable fabrication method to create nanolattices with spatially varying lattice geometry and material composition by building multilayer nanolattices with layer-by-layer control. In this technique periodic nanostructures are first patterned in photoresist by colloidal phase lithography, which is then employed as the template for atomic layer deposition (ALD) of thin oxide films. This polymer-oxide structures then form the first layer of the nanolattice stack. In addition to being the lattice material, the oxide layer also protects the underlying photoresist to enable additional lithography steps. By repeating the lithography and ALD processes, multiple nanolattices can be constructed. In this manner, different nanostructure geometry and material composition can be independently selected in each lithography and ALD step, respectively. As a demonstration of this process, a five-layer nanolattice stack over the size of 2×2 cm^2 has been fabricated. The proposed method is also employed for making a four-layer gradient-index (GRIN) antireflection stack to reduce the specular reflectance of Si wafer in 633 nm wavelength to 3%.

2. Experimental Approach

The fabrication process for the 3D nanolattice multilayer is illustrated in **Figure 1**. Initially, a monolayer of hexagonal closed-packed (HCP) polystyrene nanospheres are employed as the phase element for phase shift lithography to pattern the 3D nanostructure in photoresist,[3,19–21,23] as shown in Figure 1a. The structure can be controlled using different illumination wavelengths or nanospheres with different sizes. The patterned photoresist is then used as the sacrificial template for ALD, where a conformal thin film with desired thickness is coated, as demonstrated in Figure 1b. In a typically nanolattice process, the photoresist template is removed to result in a free-standing porous film.[1,3,7,21,27] To create a second nanolattice layer, an additional layer photoresist is spincoated to planarize the structures, as shown in Figure 1c. Note the inorganic ALD film on the first layer protects the underlying photoresist from the subsequent lithography processes. The photoresist can then be patterned by a second lithography step, as shown in Figure 1d with different exposure parameters to change the lattice geometry if desired. A second ALD layer with a different material can then coated on the photoresist, as shown in Figure 1e, generating a two-layer nanolattice structure with different lattice periods and materials. The photoresist patterning and ALD processes can be repeated for multiple nanolattice layers, each with different lattice geometry and material to create a film with arbitrary profile. Once all of the nanolattice layers have been patterned and coated with ALD, all photoresist templates can be removed using a thermal cycle with peak temperature of 550 °C, as shown in Figure 1f. This results in a free-standing, non-uniform nanolattice with spatially varying geometry and material composition along the direction normal to the substrate surface.

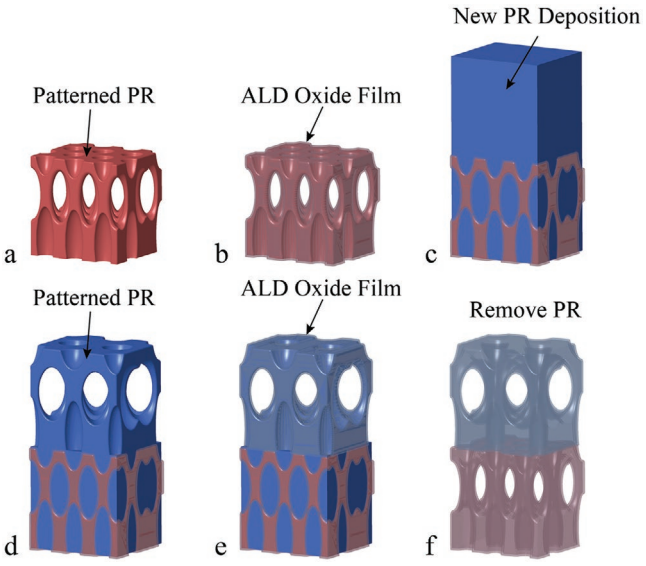

Figure 1. Schematic of non-uniform multilayer nanolattice fabrication process. a) 3D photoresist structures are patterned using colloidal phase nanolithography and used as a template for b) deposition of oxide thin films by ALD. c) A second photoresist layer is coated on the existing structures and d) patterned with desired geometry. e) ALD coating for the top photoresist layer. f) Remove the photoresist templates using thermal process to yield stacked nanolattices composed of different materials.

3. Results and Discussion

The results of fabricated non-uniform nanolattice multilayers are illustrated in **Figure 2**. A single layer of photoresist nanostructure, patterned by exposure of 350 nm-diameter polystyrene nanosphere array with a 325-nm HeCd laser, is shown in Figure 2a. The patterned photoresist is then used as a template for ALD deposition of a 25 nm-thick Al_2O_3 film. A second layer of photoresist is coated over the existing structure and lithographically patterned, as shown in Figure 2b. No air voids can be observed, indicating that the photoresist solvent is able to fully wet into the underlying ALD-coated nanostructure layer during spincoating. This is important since the photoresist can protect the first nanolattice layer from interlayer contamination by the following ALD processes. Moreover, the filled nanostructures are mechanically more stable and can prevent structure collapse often observed in solution processing of porous materials during the subsequent processes.

The interlayer bonding of different ALD coated oxides is critical in building strong multilayer nanolattices. Therefore, adequate exposure dose during lithography is important to make sure the top surface of the underlying nanolattice will be uncovered so that the following ALD film is able to bond directly on the previous ALD layer. Another consideration is the refraction index mismatch between the ALD layer and photoresist will result scattering and back-side reflection, which can induce standing waves and result in wavy photoresist sidewalls. For the oxides used in this work, the index contrast to photoresist is small and the effect is not significant. The evident of the back-side reflection can be found in

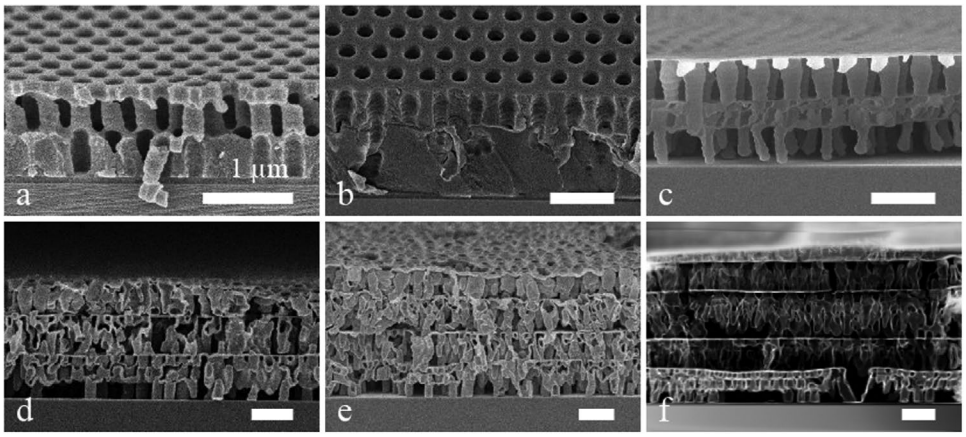

Figure 2. Cross-section scanning electron microscopy (SEM) images of the fabricated multilayer nanolattices. a) A single nanolattice layer with 350 nm period in photoresist. b) A second nanolattice layer with 500 nm period is patterned on ALD-protected underlying nanostructures. Free-standing multilayer nanolattices after photoresist removal. c) A two-layer Al_2O_3 nanolattices where the periods are 350 and 500 nm for the bottom and top layers, respectively. d) A three-layer nanolattice stack where the periods are 350, 390, and 500 nm and made by ZnO, Al_2O_3, and ZnO, respectively, from bottom to top. e) A four-layer nanolattice stack where the periods are 350, 390, 390, and 500 nm and made by ZnO, Al_2O_3, ZnO, and TiO_2, respectively, from bottom to top. f) A five-layer nanolattice stack where the periods are 350, 390, 390, 390, and 500 nm and made by ZnO, Al_2O_3, ZnO, TiO_2, and ZnO, respectively, from bottom to top. All scale bars represent 1 μm.

Figure 2c, where some wavy structures can be found on the top nanolattice layer. This can be more problematic for high-index oxides or metals, where the index contrast would be greater. In these cases, the reflection can be mitigated using an antireflection layer, which has been used to minimize reflections from silicon substrates.[21]

The fabricated two-layer nanolattice film after removal of the photoresist templates is shown in Figure 2c. The bottom nanolattice layer consists of 25-nm-thick Al_2O_3 ALD thin-shell with period of 390 nm, while the top layer is made by the same material but with period of 500 nm. The use of different sphere sizes leads to different period and unit-cell geometry by including different diffraction orders in the 3D lithography.[20] The different periods also lead to different porosity and density, which has a strong influence on the layer properties such as the optical index and mechanical stiffness.[3,21] The choice of ALD thickness and material can lead to further control of the layer properties. Moreover, the height of each nanolattice layer is determined by the photoresist thickness, which can be controlled by spin speeds during the coating process.

By repeating the lithography and ALD processes, the nanolattices can achieve arbitrary number of layers with independent geometry and material composition. Further demonstration of this process is shown in Figure 2d,f, which depicts cross-sections of three-layer, four-layer, and five-layer nanolattice stacks. For the three-layer nanolattices shown in Figure 2d, the layers from bottom to top consist of 32 nm-thick ZnO with 390 nm period, 30 nm-thick Al_2O_3 with 350 nm period, and 20 nm-thick ZnO with 500 nm period. The heights of the layers are 1100, 950, and 900 nm, respectively. For the four-layer nanolattices shown in Figure 2e, an additional 20 nm-thick TiO_2 with 650 nm period and 800 nm height are added. The five-layer nanolattices shown in Figure 2f are made by 32 nm-thick ZnO with 390 nm period, 30 nm-thick Al_2O_3 with 350 nm period, 20 nm-thick ZnO with 500 nm period, 20 nm-thick TiO_2 with 650 nm period, 20 nm-thick ZnO with 500 nm period, from bottom to top. The thicknesses of the layers are 950, 950, 1300, 850, and 800 nm, respectively.

In addition to the flexibility of the lattice geometry and layer thickness, the proposed process can also allow independent control of different ALD materials in each layer to create variations in material compositions. **Figure 3** shows are high-magnification scanning transmission electron microscopy (STEM) cross-section image of the five-layer nanolattice stack consisting of different materials shown in Figure 2f. The energy-dispersive X-ray spectroscopy (EDS) analysis of the material compositions in the nanolattice stacks is shown in Figure 3b,e. The red, green, and blue signals depict the regions which emit high intensity of radiation energy corresponding to titanium, zinc, and aluminum, respectively, demonstrating clear boundaries between the nanolattice layers. The oxygen peak is illustrated as yellow in Figure 3f, which can be detected throughout the whole nanolattice stack. It can be observed from the EDS signals that some titanium and zinc can be found below the nanolattice layer they were deposited in. This may be attributed to the overexposure during lithography, which resulted in deeper structures in the underlying layer that can be coated during the ALD process. The interlayer contamination can also be caused by the collapse of the oxide thin-shell during the cleaving process in preparation for sample characterization. Another possible source is the interlayer diffusion of the ALD deposited materials, which will be studied further in future work. The detailed energy spectra of the EDS analysis are shown in Supporting Information A.

The proposed multilayer nanolattice fabrication approach is highly versatile, and the nanolattice height, shell thickness, lattice geometry, and material composition of each layer can be independently controlled. This enables the engineering of photonic multilayers, where the effective refraction index of each layer can be precisely designed. This process is used to demonstrate GRIN stack to reduce light reflection from surfaces due to Fresnel mismatch. Using Maxwell–Garnett theory,

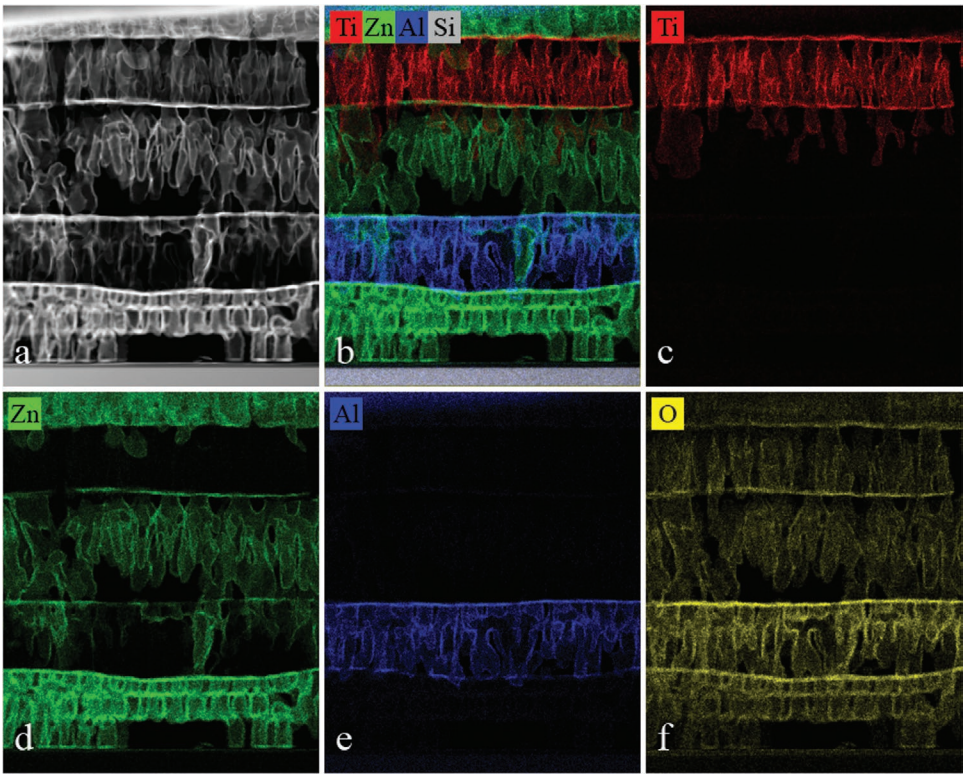

Figure 3. Cross-section STEM and EDS analysis of five-layer nanolattice structures. a) STEM image of the nanolattice stack, where the periods of each nanolattice layer from bottom to top are 350, 390, 390, 390, and 500 nm. b) The EDS analysis of the five-layer nanolattice stack made by ZnO, Al_2O_3, ZnO, TiO_2, and ZnO from bottom to top. The red, green, and blue light represents the X-ray radiation energy of titanium, zinc, and aluminum atoms. The map of peak EDS signal corresponding to c) titanium, d) zinc, e) aluminum, and f) oxygen atoms.

the effective index of each nanolattice layer can be modeled by the volume fraction and the index of the solid phase.[21,40–42] The effective index for nonmagnetic, dielectric material can be calculated by the rearranged Maxwell–Garnett equation,

$$\frac{\frac{n_{\text{eff}}^2-1}{n_{\text{eff}}^2+2}}{\frac{n_{\text{m}}^2-1}{n_{\text{m}}^2+2}} = f \tag{1}$$

where n_{m} and f are the index and volume fraction of the ALD-coated solid phase, respectively, and n_{eff} is the effective refraction index of the nanolattice layer.

The fabricated four-layer nanolattice structure on a silicon substrate with GRIN profile designed based on Equation (1) is shown in **Figure 4**. The four layers from bottom to top consist of 40-nm-thick TiO_2 with 350 nm period, 25-nm-thick TiO_2 with 390 nm period, 15-nm-thick Al_2O_3 with 390 nm period, and 15-nm-thick Al_2O_3 with 500 nm period. The heights of the layers from bottom to top are 800, 800, 1200, and 1200 nm, respectively. As the nanolattice period and shell thickness change the volume fraction, nanolattices with smaller periods and thicker shells have higher ratio of solid volume. Therefore, both the period and shell thickness of the nanolattice layers are varied to achieve the GRIN nanolattice stack. The measured refraction indices at 633 nm wavelength of each nanolattice layer are plotted along the thickness direction in Figure 4a, where the effective indices are 1.74, 1.35, 1.17, and 1.08 from bottom to top. The broadband index of each nanolattice layer is measured by spectroscopic ellipsometry (J. A. Woollam, V-VASE) over the range to 500 to 1500 nm, as shown in Figure 4b. The measurement samples consist of single nanolattice layers on silicon substrate to reduce modeling complexity. The Sellmeier model is applied for the data fitting, which is described in more detail in Supporting Information B.

The optical properties of the multilayer GRIN nanolattices on a silicon substrate are characterized, as shown in **Figure 5**, and demonstrate significant reflectance reduction. The specular reflectance of transverse electric (TE) and transverse magnetic (TM)-polarized light at 633 nm as functions of incident angle are shown in Figure 5a,b, respectively. As the number of the layers of the GRIN nanolattices stack increases to four, the specular reflectance at ≈4 degrees decreases from 35.0% to 2.9% for TE and 35.3% to 1.1% for TM mode. The antireflection effect is more dominant at large incident angle, where the reflectance decreases from 57.8% to 0.6% for TE mode and 11.8% to 0.2% for TM mode at 60 degrees. The measurement reflectance data agree well to the trend of the simulation result of the model based on rigorous coupled-wave analysis (RCWA) method.[43,44] Details of the RCWA simulation parameters are described in Supporting Information C.

The broadband specular reflectance at 15 degree incident angle for the four-layer GRIN nanolattices is characterized using a ultraviolet-visible-near-infrared (UV-vis-NIR) spectrophotometer (Agilent Cary 5000), as shown in Figure 5c. It

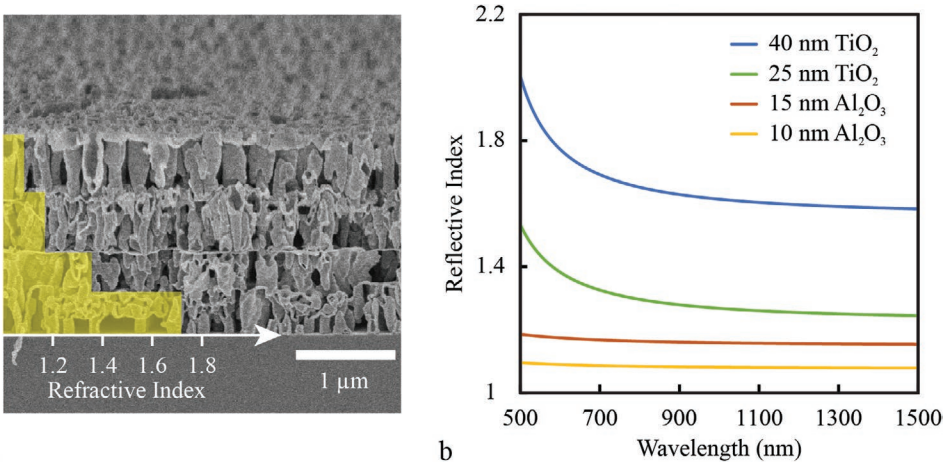

Figure 4. The four-layer GRIN nanolattice structures. a) The cross-section SEM image and the refraction index profile and b) the measured broadband refraction index of each nanolattice layer.

can be observed that the specular reflectance can be decreased to less than 6% in the range of 400 to 2400 nm wavelength. The diffuse reflectance of the GRIN nanolattice sample has also been characterized using integrating sphere detectors and shows a high peak of 42.0% at 384 nm wavelength. Details of the scattering characterization are described in Supporting Information D. The high scattering in the UV can be attributed to film roughness, local structure collapse, and assembly defects. Another reason is that the nanolattice period in this work is from 390 to 500 nm, which is not subwavelength in the UV. This leads to a peak diffused reflection in the UV, which is caused by light diffraction. This is especially critical in multilayer structures since the defects in one layer can be compounded as more layers are added. The large period relative to the wavelength can also lead to diffraction, since the nanolattice is not subwavelength in the UV. The scattering effect is more dominant compared with a single-layer nanolattice film, which peaks at 6% in the UV.[21] The optical scattering can be mitigated by using a periodic phase mask to increase the fabrication yield and reducing the nanolattice period in all layers to minimize diffraction. Nanolattices with smaller period will be investigated in the future to reduce the diffraction effects in the UV light range to reach better antireflection affect.

The proposed process has demonstrated nanolattice with non-uniform lattice geometry and material composition. Currently, the geometry and materials can only be varied along the thickness direction normal to the surface, resulting in control of the material profile in 1D. Future work will explore modifying the parameters within each individual layer, which can lead to even more complex nanolattice profiles. Currently the number of nanolattice layer that can be fabricated is limited by the yield of the nanolithography step, where the defects can be compounded when stacked. To allow more layers, the yield for each layer is important and can be improved by using lithographically patterned phase masks.[14,15,18] One future research topic could be improving the yield rate of the lithography process to achieve nanolattices with less defects and better periodicity. The demonstrated non-uniform nanolattice with varying porosity can also be applied as photonic reflector and non-uniform filter, which are areas of on-going research.

4. Conclusion

A method to fabricate non-uniform nanostructures consisting of multiple nanolattice layers has been demonstrated in this work. Using 3D near-field lithography and ALD, this process provides high versatility and independent design of lattice geometry, height, shell thickness, and material composition of each nanolattice layer. A five-layer nanolattice structure

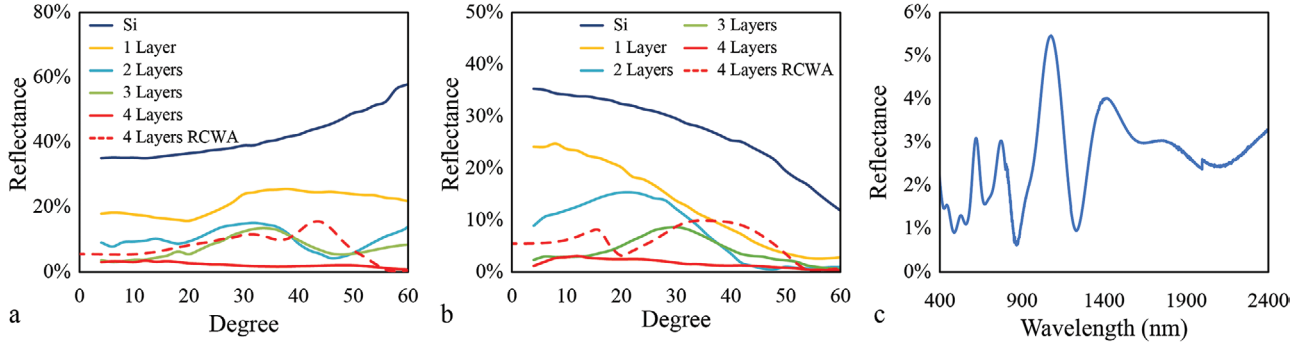

Figure 5. The optical reflectance of the GRIN nanolattices structures. The specular reflectance at 633 nm wavelength for a) TE and b) TM linearly polarized light. c) The measured broadband specular reflectance of unpolarized light for the 4-layer nanolattice sample at 15 degree incident angle.

consisting of different geometry and different oxide materials was fabricated and characterized using EDS to demonstrate clear inter-layer material boundaries. The process is also used to fabricate a four-layer GRIN antireflection structure that reduces more than 90% of specular reflectance at 633 nm wavelength and reflects less than 6% over broadband. The process can create material medium with arbitrary profile in physical properties, and can find applications in the integrated nanophotonics, optical multilayers, thermal emission control, and gradient porous filters.

5. Experimental Section

Nanolattice Fabrication: In this work the silicon substrates (100-mm single-side polished Si wafer, University Wafer) were employed after a layer of antireflection coating (ARC i-con-7, Brewer Science) with ≈100 nm thickness was applied to avoid the back reflection from the silicon substrates. A photoresist (PFi-88A2, Sumitomo) layer was then spin-coated with the thicknesses around 1 µm. The polystyrene nanospheres were applied as the periodic phase elements of the near-field lithography. The water-base suspension was first diluted with ethanol and spin-coated on a silicon wafer to achieve a monolayer of nanospheres on the substrate. The coated wafer will then immerse to water and the nanospheres will transfer to the water surface and become hexagonal-closed-packing according to capillary force. Sodium dodecyl sulfate might be used as the surfactant to accelerate the packing process. The monolayer of closed-packing monodispersed nanospheres can be transferred to the photoresist surface as the phase elements. A 325 nm HeCd laser was employed as the light source of the lithography.

Al_2O_3, TiO_2, or ZnO thin films were then coated on the polymer template with ALD process by a custom made vacuum reactor with viscous-flow, hot-walled ALD system.[45–47] Two self-limiting half reactions were included in ALD process to yield a conformal thin film on the template surface. High purity nitrogen gas (Machin & Welding Supply Co) which was further purified with an Entegris GateKeeper was employed to purge the reactor after the termination of each self-limiting half reaction. Trimethyl aluminum (TMA, Strem Chemicals, min 98%) was employed as the metal-containing precursor and co-reacted with deionized water with the recipe 1/30/1/60 (TMA dose/nitrogen purge/water dose/nitrogen purge, in seconds) for Al_2O_3 deposition with the growth rate of 1.1 Å per ALD cycle under the condition of 550 mTorr and 90 °C. Diethyl zinc (DEZ, Strem Chemicals, min 98%) was employed as the precursor to react with deionized water to deposit ZnO under the growth rate of 1.6 Å per DEZ/Water ALD cycle. To monitor the film growth and thickness, a silicon wafer (University Wafers, P-type, <1 0 0>) was placed in the front and back of the reactor chamber as the reference sample and further examined by an α-SE ellipsometer (J.A. Woollam Co., Inc) to determine the film thickness.

Supporting Information

Supporting Information is available from the Wiley Online Library or from the author.

Acknowledgements

This work was in part performed at the NCSU Nanofabrication Facility (NNF) and the Analytical Instrumentation Facility (AIF), members of the North Carolina Research Triangle Nanotechnology Network (RTNN), which is supported by the National Science Foundation as part of the National Nanotechnology Coordinated Infrastructure (NNCI) grant NNCI-2025064, and at the UT Austin Texas Materials Institute (TMI), the Nanomanufacturing System for mobile Computing and Energy Technologies (NASCENT), and Texas Nanofabrication Facilities, which is supported by the National Science Foundation as part of the National Nanotechnology Coordinated Infrastructure (NNCI) grant NNCI-2025227. This work was supported by the National Science Foundation (NSF) under grant CMMI#1552424. This article has been amended on September 9, 2021 to add D. T. Lee as the third author.

Conflict of Interest

The authors declare no conflict of interest.

Data Availability Statement

Data available on request from the authors.

Keywords

3D nanostructures, antireflection structures, nanoarchitected materials, nanolattices

Received: April 28, 2021
Revised: June 15, 2021
Published online: July 26, 2021

[1] L. R. Meza, S. Das, J. R. S. Greer, *Science* **2014**, *345*, 1322.
[2] T. A. Schaedler, A. J. Jacobsen, A. Torrents, A. E. Sorensen, J. Lian, J. R. Greer, L. Valdevit, W. B. Carter, *Science* **2011**, *334*, 962.
[3] A. Bagal, X. A. Zhang, R. Shahrin, E. C. Dandley, J. Zhao, F. R. Poblete, C. J. Oldham, Y. Zhu, G. N. Parsons, C. Bobko, C.-H. Chang, *Sci. Rep.* **2017**, *7*, 9145.
[4] X. Zheng, H. Lee, T. H. Weisgraber, M. Shusteff, J. DeOtte, E. B. Duoss, J. D. Kuntz, M. M. Biener, Q. Ge, J. A. Jackson, S. O. Kucheyev, N. X. Fang, C. M. Spadaccini, *Science* **2014**, *344*, 1373.
[5] J.-H. Lee, L. Wang, S. Kooi, M. C. Boyce, E. L. Thomas, *Nano Lett.* **2010**, *10*, 2592.
[6] J. Bauer, S. Hengsbach, I. Tesari, R. Schwaiger, O. Kraft, *Proc. Natl. Acad. Sci. USA* **2014**, *111*, 2453.
[7] D. Jang, L. R. Meza, F. Greer, J. R. Greer, *Nat. Mater.* **2013**, *12*, 893.
[8] D. R. Rolison, J. W. Long, J. C. Lytle, A. E. Fischer, C. P. Rhodes, T. M. McEvoy, M. E. Bourg, A. M. Lubers, *Chem. Soc. Rev.* **2008**, *38*, 226.
[9] Y.-G. Guo, J.-S. Hu, L.-J. Wan, *Adv. Mater.* **2008**, *20*, 2878.
[10] Q. Zhang, E. Uchaker, S. L. Candelaria, G. Cao, *Chem. Soc. Rev.* **2013**, *42*, 3127.
[11] E. Yablonovitch, *Phys. Rev. Lett.* **1987**, *58*, 2059.
[12] T. Gorishnyy, C. K. Ullal, M. Maldovan, G. Fytas, E. L. Thomas, *Phys. Rev. Lett.* **2005**, *94*, 115501.
[13] G. v. Freymann, A. Ledermann, M. Thiel, I. Staude, S. Essig, K. Busch, M. Wegener, *Adv. Funct. Mater.* **2010**, *20*, 1038.
[14] S.-H. Nam, J. Park, S. Jeon, *Adv. Funct. Mater.* **2019**, *29*, 1904971.
[15] S. H. Nam, G. Hyun, D. Cho, S. Han, G. Bae, H. Chen, K. Kim, Y. Ham, J. Park, S. Jeon, *Nano Res.* **2021**. https://doi.org/10.1007/s12274-021-3428-6.
[16] M. Campbell, D. N. Sharp, M. T. Harrison, R. G. Denning, A. J. Turberfield, *Nature* **2000**, *404*, 53.
[17] L. Wu, Y. Zhong, C. T. Chan, K. S. Wong, G. P. Wang, *Appl. Phys. Lett.* **2005**, *86*, 241102.
[18] S. Jeon, J.-U. Park, R. Cirelli, S. Yang, C. E. Heitzman, P. V. Braun, P. J. A. Kenis, J. A. Rogers, *Proc. Natl. Acad. Sci. USA* **2004**, *101*, 12428.

[19] C.-H. Chang, L. Tian, W. R. Hesse, H. Gao, H. J. Choi, J.-G. Kim, M. Siddiqui, G. Barbastathis, *Nano Lett.* **2011**, *11*, 2533.
[20] J.-H. Min, X. A. Zhang, C.-H. Chang, *Opt. Express* **2016**, *24*, A276.
[21] X. A. Zhang, A. Bagal, E. C. Dandley, J. Zhao, C. J. Oldham, B.-I. Wu, G. N. Parsons, C.-H. Chang, *Adv. Funct. Mater.* **2015**, *25*, 6644.
[22] X. Zhang, I.-T. Chen, C.-H. Chang, *Nanotechnology* **2019**, *30*, 352002.
[23] I.-T. Chen, E. Schappell, X. Zhang, C.-H. Chang, *Microsyst. Nanoeng.* **2020**, *6*, 22.
[24] O. D. Velev, E. W. Kaler, *Adv. Mater.* **2000**, *12*, 531.
[25] M. Fang, H. Lin, H.-Y. Cheung, F. Xiu, L. Shen, S. Yip, E. Y.-B. Pun, C.-Y. Wong, J. C. Ho, *ACS Appl. Mater. Interfaces* **2014**, *6*, 20837.
[26] X. Liang, R. Dong, J. C. Ho, Self-Assembly of Colloidal Spheres toward Fabrication of Hierarchical and Periodic Nanostructures for Technological Applications, https://onlinelibrary.wiley.com/doi/abs/10.1002/admt.201800541 (accessed: July 2019).
[27] N. G. Dou, R. A. Jagt, C. M. Portela, J. R. Greer, A. J. Minnich, *Nano Lett.* **2018**, *18*, 4755.
[28] D. Brownlee, P. Tsou, J. Aléon, C. M. O'D. Alexander, T. Araki, S. Bajt, G. A. Baratta, R. Bastien, P. Bland, P. Bleuet, J. Borg, J. P. Bradley, A. Brearley, F. Brenker, S. Brennan, J. C. Bridges, N. D. Browning, J. R. Brucato, E. Bullock, M. J. Burchell, H. Busemann, A. Butterworth, M. Chaussidon, A. Cheuvront, M. Chi, M. J. Cintala, B. C. Clark, S. J. Clemett, G. Cody, L. Colangeli, G. Cooper, P. Cordier, C. Daghlian, Z. Dai, L. D'Hendecourt, et al., *Science* **2006**, *314*, 1711.
[29] S. A. Sandford, J. Aléon, C. M. O. Alexander, T. Araki, S. Bajt, G. A. Baratta, J. Borg, J. P. Bradley, D. E. Brownlee, J. R. Brucato, M. J. Burchell, H. Busemann, A. Butterworth, S. J. Clemett, G. Cody, L. Colangeli, G. Cooper, L. D'Hendecourt, Z. Djouadi, J. P. Dworkin, G. Ferrini, H. Fleckenstein, G. J. Flynn, I. A. Franchi, M. Fries, M. K. Gilles, D. P. Glavin, M. Gounelle, F. Grossemy, C. Jacobsen, L. P. Keller, A. L. D. Kilcoyne, J. Leitner, G. Matrajt, A. Meibom, et al., *Science* **2006**, *314*, 1720.
[30] J.-H. Jang, C. K. Ullal, T. Choi, M. C. Lemieux, V. V. Tsukruk, E. L. Thomas, *Adv. Mater.* **2006**, *18*, 2123.
[31] T. Ergin, N. Stenger, P. Brenner, J. B. Pendry, M. Wegener, *Science* **2010**, *328*, 337.
[32] T. Bückmann, M. Thiel, M. Kadic, R. Schittny, M. Wegener, *Nat. Commun.* **2014**, *5*, 4130.
[33] N. Yu, F. Capasso, *Nat. Mater.* **2014**, *13*, 139.
[34] M. Khorasaninejad, W. T. Chen, R. C. Devlin, J. Oh, A. Y. Zhu, F. Capasso, *Science* **2016**, *352*, 1190.
[35] C. Zheng, Y. Shen, M. Liu, W. Liu, S. Wu, C. Jin, *ACS Nano* **2019**, *13*, 5583.
[36] A. A. Patel, H. I. Smith, *J. Vac. Sci. Technol., B: Microelectron. Nanometer Struct.–Process., Meas., Phenom.* **2007**, *25*, 2662.
[37] K. Aoki, H. T. Miyazaki, H. Hirayama, K. Inoshita, T. Baba, N. Shinya, Y. Aoyagi, *Appl. Phys. Lett.* **2002**, *81*, 3122.
[38] J. Jeon, H. C. Floresca, M. J. Kim, *J. Vac. Sci. Technol., B: Microelectron. Nanometer Struct.–Process., Meas., Phenom.* **2010**, *28*, 549.
[39] D. Chen, X. Zheng, *Sci. Rep.* **2018**, *8*, 9139.
[40] J. C. M. Garnett, *Philos. Trans. R. Soc., A* **1904**, *203*, 385.
[41] N. J. Hutchinson, T. Coquil, A. Navid, L. Pilon, *Thin Solid Films* **2010**, *518*, 2141.
[42] P. Sarafis, A. G. Nassiopoulou, *Nanoscale Res. Lett.* **2014**, *9*, 418.
[43] M. G. Moharam, T. K. Gaylord, E. B. Grann, D. A. Pommet, *J. Opt. Soc. Am. A* **1995**, *12*, 1068.
[44] M. G. Moharam, T. K. Gaylord, D. A. Pommet, E. B. Grann, *J. Opt. Soc. Am. A* **1995**, *12*, 1077.
[45] B. Gong, Q. Peng, J. S. Jur, C. K. Devine, K. Lee, G. N. Parsons, *Chem. Mater.* **2011**, *23*, 3476.
[46] J. C. Spagnola, B. Gong, S. A. Arvidson, J. S. Jur, S. A. Khan, G. N. Parsons, *J. Mater. Chem.* **2010**, *20*, 4213.
[47] J. S. Jur, J. C. Spagnola, K. Lee, B. Gong, Q. Peng, G. N. Parsons, *Langmuir* **2010**, *26*, 8239.